

Ejection of innershell electrons induced by recollision in a laser-driven carbon atomErik Lötstedt^{1,2,3,*} and Katsumi Midorikawa^{1,2}¹*Laser Technology Laboratory, RIKEN, 2-1 Hirosawa, Wako, Saitama 351-0198, Japan*²*RIKEN Center for Advanced Photonics, 2-1 Hirosawa, Wako, Saitama 351-0198, Japan*³*Department of Chemistry, School of Science, The University of Tokyo, 7-3-1 Hongo, Bunkyo-ku, Tokyo 113-0033, Japan*

(Received 3 September 2014; published 23 October 2014)

Ejection of core electrons as a result of recollision in a laser-driven carbon atom is theoretically investigated with a quasiclassical model. The model, called “fermionic molecular dynamics,” gives rise to a ground-state carbon atom where the six electrons are paired in shells, with different binding energies. This feature renders possible, on a classical level, the discussion of the ejection of electrons from different shells. By analyzing a large number of trajectories of a carbon atom exposed to an intense, few-cycle laser pulse, we reveal a class of recollision trajectories where the recolliding electron is recaptured into the atomic core after ejecting a core electron. We also discuss the difference between quadruple ionization trajectories leading to a final C^{4+} ion where the two bound electrons have opposite spin, and the trajectories where the bound electrons have equal spin.

DOI: [10.1103/PhysRevA.90.043415](https://doi.org/10.1103/PhysRevA.90.043415)

PACS number(s): 32.80.Aa, 34.10.+x, 33.80.Wz, 02.70.Ns

I. INTRODUCTION

Many-electron atoms exposed to intense laser light behave in a complex way. Intense means here laser pulses of intensity larger than 10^{14} W/cm², and we have near-infrared (typically 800 nm) light in mind. Individual electrons can absorb energy from the light field, and subsequently redistribute this energy to other bound electrons through electron-electron interaction. A prominent example is the nonsequential double ionization (NSDI) process [1–6]. In NSDI, one electron is first ejected by field ionization, and then accelerated by the driving laser field so as to recollide [7,8] with the residual ionic core at a kinetic energy sufficiently high to knock out also a second electron.

Even more exciting is the possibility for more than one electron to be simultaneously ejected by the recolliding electron, creating a multiply charged ion in the final state. Although there is ample experimental evidence for nonsequential multiple ionization (NSMI) [9–18], a detailed theoretical understanding is lacking.

In general, the theoretical description of a laser-driven many-electron atom can be considered to be an open problem. Numerically exact solutions to the time-dependent Schrödinger equation for laser-driven atoms have so far been obtained only for helium [19]. Even though there exist promising approximate approaches such as time-dependent density functional theory [20–23], time-dependent multiconfiguration methods [24–30], and R -matrix theory [31–33], complete quantum mechanical calculations where more than two electrons are actively driven by the laser field seem to be beyond current capabilities.

An interesting alternative to quantum mechanical methods is to use classical mechanics. The coupled, classical equations of motion can be easily solved, including both the force exerted by the laser field on the electrons as well as the interelectronic Coulomb force. This means that within the classical approximation, electron correlation is treated exactly. Arguably, the largest advantage of classical

methods is that once a large number of trajectories have been calculated, the analysis of the various physical mechanisms involved is straightforward, and often leads to valuable insight.

Classical trajectory methods applied to the NSDI process can be broadly divided into two classes, depending on how the initial conditions are treated. In the first class [34–50], the initial momenta and positions for the bound electrons are sampled from a microcanonical ensemble with fixed total energy, as pioneered by Abrines and Percival [51]. In this approach autoionization is avoided by a regularization of the short-distance electron-nucleus interaction, usually by employing a soft-core potential $V(\mathbf{r}) = -Ze^2/\sqrt{\mathbf{r}^2 + \alpha^2}$ instead of the Coulomb potential. Classical calculations in this class have also provided a promising attack on the nonsequential triple ionization problem [46,47,52–54]. A second class of methods [55–58] derives the initial velocity for the ejected electron from the probability distribution that follows from quantum mechanical tunneling ionization [59].

In this article, we employ another type of classical model, termed “fermionic molecular dynamics” (FMD), to study the response of a carbon atom exposed to an intense laser pulse. In this model, originally suggested in [60,61], electrons are treated as classical point particles, but in addition to the Coulomb potential, the electron-nucleus interaction is augmented by a momentum-dependent potential that prevents the electron from visiting parts of the classical phase space that would be forbidden in quantum mechanics. In addition, a similar auxiliary repulsive potential acting between electrons with equal spin is introduced, which makes it possible to describe multielectron atoms. Since the interparticle potentials depend on both the position and the momentum of the particles, the FMD model is referred to as quasiclassical. The FMD model has been shown to produce stable, quasiclassical ground-state configurations for all atoms with charge number $Z \leq 94$ [62,63], and has been applied extensively to atomic and molecular collisions [64–72]. Beginning with the application to laser-driven helium [73,74], it has also been successfully used for the description of laser-atom interaction [75–79], laser-molecule interaction [80–83], and laser-cluster

*lotstedt@chem.s.u-tokyo.ac.jp

interaction [84]. We mention that in [84], where the FMD model was also used to simulate the laser-driven dynamics of the six valence electrons in a single Xe atom, good qualitative agreement with experimentally measured ionization yields was found.

By employing the FMD model, we show that an increased understanding of NSMI in a laser-driven carbon atom can be obtained. We are particularly interested in the ejection of tightly bound core electrons by a recolliding electron. One of the most interesting findings of the current investigation is a class of trajectories where the recolliding electron is recaptured into a core hole formed by a previously ejected core electron. This illustrates the main strength of the classical trajectory approach: the ability to find qualitatively new paths contributing to a physical process. However, due to the rather drastic approximations involved in describing a complex quantum object such as a many-electron atom with a quasiclassical model, we do not expect the model to be able to produce results that agree quantitatively with experimental measurements.

We organize the paper as follows. In Sec. II, we introduce the FMD model. The properties of the ground state of a C atom as described by the FMD model are investigated in Sec. II B. Our results of the Monte Carlo simulations are presented and discussed in Sec. III, with special emphasis being put on the trajectories leading to quadruple ionization (Secs. III B and III C). Section IV concludes the paper.

II. THEORETICAL MODEL

A. Basic equations

The FMD model is based on the Hamiltonian formulation of classical dynamics. The total, laser-field-free Hamiltonian H for N electrons bound to a nucleus with charge number Z is defined by [61,66]

$$H = \frac{\mathbf{P}^2}{2M} + \sum_{i=1}^N \left[\frac{\mathbf{p}_i^2}{2} - \frac{Z}{\rho_i} + \frac{f(Q_i, \rho_i, \xi_0)}{\mu \rho_i^2} \right] + \frac{1}{2} \sum_{\substack{i,j=1 \\ i \neq j}}^N \left[\frac{1}{r_{ij}} + \delta_{\sigma_i \sigma_j} \frac{2f(q_{ij}, r_{ij}, \eta_0)}{r_{ij}^2} \right], \quad (1)$$

where the position, momentum, and spin of electron i are denoted by \mathbf{r}_i , \mathbf{p}_i , and σ_i , respectively, \mathbf{R} is the position of the nucleus, \mathbf{P} is the momentum of the nucleus, M is the nuclear mass, $\mu = M/(M+1)$, and we have used the abbreviations $Q_i = |\mathbf{P} - M\mathbf{p}_i|/(M+1)$, $\rho_i = |\mathbf{r}_i - \mathbf{R}|$, $q_{ij} = |\mathbf{p}_i - \mathbf{p}_j|/2$, and $r_{ij} = |\mathbf{r}_i - \mathbf{r}_j|$. Atomic units (a.u.) are used, as throughout this paper, unless otherwise stated. In the calculations below, we restrict our attention to the carbon atom, and fix $Z = N = 6$, and $M = 12 \times 1836 = 22032$ a.u. The spin $\sigma_i \in \{\alpha, \beta\}$ is fixed for each electron, and only electrons with the same spin (α or β) interact via the last term in Eq. (1). The auxiliary function f , used to implement the classical phase-space constraints, is defined as [61,66]

$$f(q, r, \xi) = \frac{\xi^2}{16} \exp\{4[1 - (qr/\xi)^4]\}. \quad (2)$$

We follow [61] and put $\xi_0 = 1/\sqrt{1+1/8} \approx 0.94$ and $\eta_0 = 2.767/\sqrt{1+1/8} \approx 2.61$ for the constants ξ_0 and η_0 in Eq. (1).

The equations of motion governing the dynamics follow from the Hamiltonian H as

$$\begin{aligned} \frac{d\mathbf{r}_i}{dt} &= \frac{\partial H}{\partial \mathbf{p}_i}, & \frac{d\mathbf{p}_i}{dt} &= -\frac{\partial H}{\partial \mathbf{r}_i} - \mathbf{E}(t, \mathbf{r}_i) - \frac{d\mathbf{r}_i}{dt} \times \frac{\mathbf{B}(t, \mathbf{r}_i)}{c}, \\ \frac{d\mathbf{R}}{dt} &= \frac{\partial H}{\partial \mathbf{P}}, & \frac{d\mathbf{P}}{dt} &= -\frac{\partial H}{\partial \mathbf{R}} + Z \left[\mathbf{E}(t, \mathbf{R}) + \frac{d\mathbf{R}}{dt} \times \frac{\mathbf{B}(t, \mathbf{R})}{c} \right], \end{aligned} \quad (3)$$

where c is the speed of light, and where we have introduced the electric field $\mathbf{E}(t, \mathbf{r})$ and the magnetic field $\mathbf{B}(t, \mathbf{r})$ of the laser pulse. The explicit form adopted for the laser field is

$$\begin{aligned} \mathbf{E}(t, \mathbf{r}) &= \hat{\mathbf{x}} E_0 \Psi(t - z/c), & \mathbf{B}(t, \mathbf{r}) &= \hat{\mathbf{z}} \times \mathbf{E}(t, \mathbf{r}), \\ \Psi(\tau) &= \begin{cases} \cos(\omega_0 \tau + \varphi_0) \sin^2\left(\frac{\pi \tau}{T_0}\right) & \text{if } 0 \leq \tau \leq T_0, \\ 0 & \text{otherwise.} \end{cases} \end{aligned} \quad (4)$$

The laser field is characterized by the peak field strength E_0 , the angular frequency ω_0 , the carrier-envelope phase (CEP) φ_0 , and the pulse length $T_0 = 2\pi n_c / \omega_0$, where n_c is the number of optical cycles. The magnetic field of the laser pulse is included since the $(d\mathbf{r}/dt) \times \mathbf{B}$ force was shown in [49] to have a non-negligible effect on the recollision process already at laser intensities of 10^{15} W/cm².

Reviews of the FMD model can be found in [85,86], and we limit ourselves to a few brief comments about the Hamiltonian H (1) and the resulting equations of motion (3). Since the potential depends on the momentum of the particles, we have in general $d\mathbf{r}_i/dt \neq \mathbf{p}_i$. However, due to the exponential character of the function f [see Eq. (2)], this inequality holds only for small interparticle separations or small relative momenta. At large distances or momenta we recover the usual situation where $d\mathbf{r}_i/dt = \mathbf{p}_i$. It is worth pointing out that in the absence of a laser field, Eq. (3) implies that both energy and momentum are conserved: $dH(t)/dt = 0$ and $(d/dt)[\sum_i \mathbf{p}_i(t) + \mathbf{P}(t)] = 0$. For a nonvanishing laser field, due to the property $\int_0^{T_0} \Psi(\tau) d\tau = 0$, we still have momentum conservation in the x direction after the laser pulse, $\hat{\mathbf{x}} \cdot [\sum_i \mathbf{p}_i(-\infty) + \mathbf{P}(-\infty)] = \hat{\mathbf{x}} \cdot [\sum_i \mathbf{p}_i(\infty) + \mathbf{P}(\infty)]$. In the z direction (the propagation direction of the laser pulse) there can be a net gain of momentum in general; this corresponds to the absorption of photon momentum. In fact, we have $dH/dt = -\sum_i (d\mathbf{r}_i/dt) \cdot \mathbf{E}(t, \mathbf{r}_i) + (d\mathbf{R}/dt) \cdot \mathbf{E}(t, \mathbf{R}) = c\hat{\mathbf{z}} \cdot (\sum_i d\mathbf{p}_i/dt + d\mathbf{P}/dt)$, so that $H(\infty) - H(-\infty) = c\hat{\mathbf{z}} \cdot [\sum_i \mathbf{p}_i(\infty) + \mathbf{P}(\infty)]$ (assuming vanishing total momentum at $t = -\infty$).

Another important observation is that H is invariant under separate rotations of all position vectors and all momentum vectors [61,62]. This means that

$$\begin{aligned} H(\mathbf{r}_1, \dots, \mathbf{r}_N, \mathbf{R}, \mathbf{p}_1, \dots, \mathbf{p}_N, \mathbf{P}) \\ = H(\Omega_1 \mathbf{r}_1, \dots, \Omega_1 \mathbf{r}_N, \Omega_1 \mathbf{R}, \Omega_2 \mathbf{p}_1, \dots, \Omega_2 \mathbf{p}_N, \Omega_2 \mathbf{P}), \end{aligned} \quad (5)$$

where Ω_1 and Ω_2 are two different rotation matrices. This fact is used in the simulation to generate random initial conditions which share the same total energy.

B. Ground state

The ground state of the model C atom is defined as the particle configuration which minimizes the value of the Hamiltonian H . In the stationary ground-state configuration, the particles do not move, $d\mathbf{r}_i^{(g)}/dt = \mathbf{0}$, but in general the momentum is nonzero, $\mathbf{p}_i^{(g)} \neq \mathbf{0}$. By employing the minimization algorithm described in [87] (see also the implementation in [88]), we have found that the minimum energy of H is given by a configuration where the six electrons have alternating spin (three α and three β electrons), and where the electrons are located in a plane, pairwise arranged around the C nucleus. The ground-state configuration is illustrated in Fig. 1(a). The energy of the ground state was found to be $\mathcal{E}_0 = -43.3762$ a.u. This value, and the positions and momenta of the electrons in the ground state, are consistent with the results presented in [62,63]. For comparison, the energy of a higher spin state, where four electrons have α spin, and two β spin, was calculated to be $\mathcal{E}_0 = -43.0707$ a.u.

We have also calculated the lowest-energy configurations of the ions C^{n+} , $n = 1, 2, \dots, 5$, using the Hamiltonian (1) with

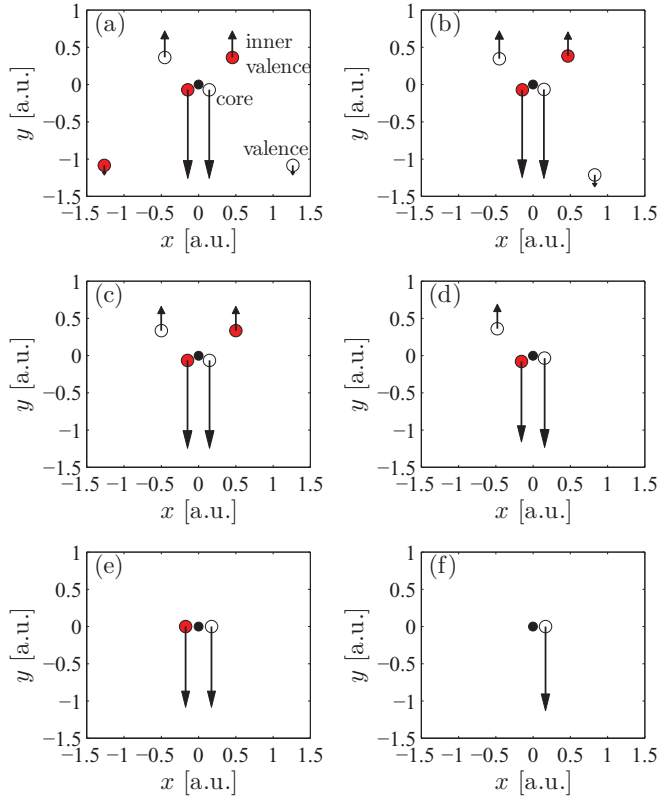


FIG. 1. (Color online) Coordinates $\mathbf{r}_i^{(g)}$ of the electrons in the FMD ground state of (a) neutral C, (b) C^+ , (c) C^{2+} , (d) C^{3+} , (e) C^{4+} , and (f) C^{5+} . In all panels, all electrons are located in the xy plane. α spin electrons are shown with red, solid circles, β electrons are shown with open circles, and the C nucleus is shown as a slightly smaller, black solid circle. The arrows indicate the direction and magnitude of the momenta $\mathbf{p}_i^{(g)}$ (all lying in the xy plane) in the ground state; the scale for the momentum vectors is set by the value $|\mathbf{p}_{\text{core}}^{(g)}| \approx 5.95$ a.u. for neutral C [the longest momentum vectors in (a)]. Not shown is the momentum $\mathbf{P}^{(g)}$ of the C nucleus, which is $\mathbf{P}^{(g)} \approx (0, 9.63, 0)$ a.u. for neutral C, and similar for the other charge states.

$N = 6 - n$. The results are shown in Figs. 1(b)–1(f). The ionic ground-state configurations are all similar to the case of neutral C. In particular, all ground-state configurations were found to be planar. The even-electron ions (C , C^{2+} , and C^{4+}) are symmetric, while the odd-electron ions (C^+ , C^{3+} , and C^{5+}) are slightly asymmetric. We have confirmed that all ground-state configurations are stable by running simulations (without the laser field) starting from the momenta and positions as shown in Figs. 1(a)–1(f), and checking that autoionization does not occur.

An interesting feature of the quasiclassical ground state of atoms in the FMD model is that the electrons form “shells” [62], in the sense that some electrons are located close to the nucleus, with high value of the momentum, while others (“valence electrons”) are situated farther away, and have smaller momentum. The shell structure for the C atom considered in the current investigation can be clearly seen in Fig. 1. Another way of quantifying how deeply bound the different electrons are is to define a single-electron energy ϵ_i as

$$\begin{aligned} \epsilon_i &= \epsilon_i^{(\text{kin})} + \epsilon_i^{(\text{pot})} + \epsilon_i^{(\text{aux})} + \frac{1}{2}\epsilon_i^{(2e)}, \\ \epsilon_i^{(\text{kin})} &= \frac{\mathbf{p}_i^2}{2}, \quad \epsilon_i^{(\text{pot})} = -\frac{Z}{\rho_i}, \quad \epsilon_i^{(\text{aux})} = \frac{f(Q_i, \rho_i, \xi_0)}{\mu\rho_i^2}, \\ \epsilon_i^{(2e)} &= \sum_{\substack{j=1 \\ j \neq i}}^N \left[\frac{1}{r_{ij}} + \delta_{\sigma_i\sigma_j} \frac{2f(q_{ij}, r_{ij}, \eta_0)}{r_{ij}^2} \right], \end{aligned} \quad (6)$$

which satisfies $\sum_{i=1}^6 \epsilon_i = H - \mathbf{P}^2/2M$. For the ground-state configuration of neutral C shown in Fig. 1(a), we have $\epsilon_{\text{val}} \approx -2.01$ a.u. for the two valence electrons farthest away from the nucleus, $\epsilon_{\text{ival}} \approx -5.83$ a.u. for the next pair of inner valence electrons, and $\epsilon_{\text{core}} \approx -13.84$ a.u. for the two core electrons. The single-electron energy ϵ_i as defined in Eq. (6) is the appropriate one if all electrons are actively responding to the laser field [62,75]. In the limiting case where only one electron is active, it is more suitable to define the single-electron energy as

$$\tilde{\epsilon}_i = \epsilon_i^{(\text{kin})} + \epsilon_i^{(\text{pot})} + \epsilon_i^{(\text{aux})} + \epsilon_i^{(2e)}, \quad (7)$$

i.e., without the factor of 1/2 in front of the two-electron terms [62,75]. The alternative single-electron energy $\tilde{\epsilon}_i$ corresponds to an approximate ionization energy, comparable to Koopmans’ theorem [89] in quantum chemistry: $-\tilde{\epsilon}_i$ is the energy required to remove electron i to infinity when all other electrons are frozen. In the analysis of the laser-driven dynamics presented in Sec. III, we will use the single-electron energy (6).

We note that the symmetry (5) implies that the total angular momentum $\mathbf{L} = \sum_i \mathbf{r}_i \times \mathbf{p}_i + \mathbf{R} \times \mathbf{P}$ is not fixed for a given ground-state configuration. For example, even though the particle configuration in Fig. 1(a) is plotted with momentum vectors such that $\mathbf{L} = \mathbf{0}$, equivalent configurations with the same total energy, but a nonzero $|\mathbf{L}|$, can be constructed by simultaneous rotation of all momentum vectors.

As a further characterization of the C atom as described by the FMD model, we have calculated the ionization potentials

TABLE I. Comparison of IPs obtained experimentally (Expt.), by Hartree-Fock calculations (HF), and by the FMD model. The column labeled by the Roman numeral n indicates the energy in a.u., rounded to two decimal places, required to ionize $C^{(n-1)+} \rightarrow C^{n+}$. The HF values were calculated with GAMESS [90], using the 6-311G basis set. Experimental values are taken from [91]. For comparison, also the value $-\tilde{\epsilon}_v$ [see Eq. (7)] of the outermost valence electron v of $C^{(n-1)+}$ is included in the table.

	I	II	III	IV	V	VI
Expt.	0.41	0.90	1.76	2.37	14.41	18.01
HF	0.40	0.88	1.68	2.36	14.37	17.99
FMD	0.55	1.02	3.95	4.79	15.06	18.00
$-\tilde{\epsilon}_v$	0.63	1.12	4.14	5.14	15.10	18.00

(IPs) of the neutral C atom as well as of its ions. The results are shown in Table I. The IP of the ion C^{n+} is calculated by the difference in ground-state energy between $C^{(n+1)+}$ and C^{n+} . The values of the IPs obtained by the FMD model are quantitatively different compared to the corresponding experimental values, but do reproduce the qualitative trend with increasing charge.

III. RESULTS

In this section we describe the results of the model C atom exposed to an intense, long-wavelength, few-cycle laser pulse. Throughout this section, we use $\omega_0 = 0.057$ a.u. (corresponding to a wavelength of 800 nm), $\varphi_0 = 0$, and $n_c = 3$ (corresponding to a total pulse width T_0 of approximately 331 a.u. = 7.9 fs) for the parameters of the laser pulse. The simulations are conducted by the Monte Carlo method: a large number of trajectories with different initial conditions are simulated by numerically solving the equations of motion (3) using a fifth-order, adaptive Runge-Kutta solver. The simulation covers the interval $0 \leq t \leq t_{\text{tot}}$, with $t_{\text{tot}} = 1.5T_0$. The initial values for the particle positions and momenta are taken as

$$\mathbf{r}_i(0) = \Omega_1 \mathbf{r}_i^{(g)}, \quad \mathbf{p}_i(0) = \Omega_2 \mathbf{p}_i^{(g)}, \quad \mathbf{P}(0) = \Omega_2 \mathbf{P}^{(g)}, \quad (8)$$

and $\mathbf{R}(0) = \mathbf{0}$, where $\Omega_{1,2}$ are two different random rotation matrices (different for each run), and $\mathbf{r}_i^{(g)}$, $\mathbf{p}_i^{(g)}$, and $\mathbf{P}^{(g)}$ refer to the ground-state configuration shown in Fig. 1(a). After running many trajectories, ionization probabilities P_n are calculated as $P_n = k_n/k_{\text{tot}}$, where k_n is the number of ionization events with final charge state n and k_{tot} is the total number of trajectories simulated. An electron i is assumed to be ejected if $\epsilon_i > 0$ [see Eq. (6) for definition] at the end of the simulation.

We note that since the present model treats the electrons as classical point particles, wave-packet spreading of a single ejected electron is not taken into account. However, since we simulate many trajectories with different initial conditions (positions and momenta), the total ensemble of trajectories of the ejected electron does exhibit phase-space spreading.

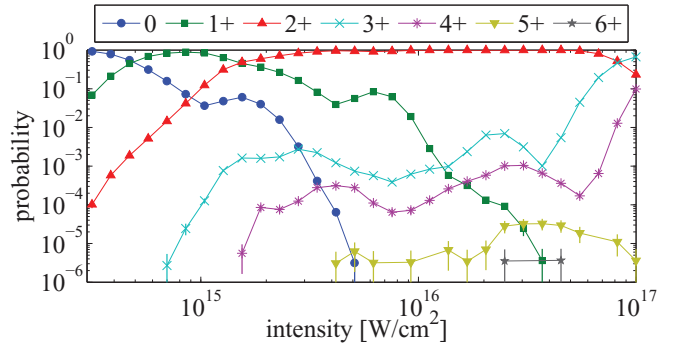


FIG. 2. (Color online) Total probability P_n to ionize to different final charge states, as indicated in the legend (the line labeled by $n+$ indicates that n electrons were ejected), as a function of the laser intensity. Statistical error bars $\pm\sqrt{k_n}/k_{\text{tot}}$ (\pm one standard deviation) are shown when their length exceeds the size of the curve symbols.

A. Total probabilities for all ionization channels

In Fig. 2 we show the total ionization probability as a function of the laser intensity, for intensities $I \geq 10^{14}$ W/cm². Intensity is related to the field strength in a.u. by the formula I [W cm⁻²] = $3.51 \times 10^{16} E_0^2$ [a.u.]. About $k_{\text{tot}} = 3 \times 10^5$ trajectories were run at each value of the intensity. For intensities below 10^{15} W/cm², the dominating channel is single ionization, while the majority of events above 10^{15} W/cm² are double ionization. At the intensity of about 4×10^{14} W/cm², there is a slight kink in the double-ionization curve (red curve with \blacktriangle symbols), hinting at the occurrence of NSDI [4–8,34–50]. We have checked that at 4×10^{14} W/cm², the events where two electrons are ejected are indeed caused by recollision.

The most interesting channels are triple, quadruple, and quintuple ionization. For the events where all six electrons were ejected, the statistics are not good enough to make any conclusive statement. The three curves in Fig. 2 where 3, 4, or 5 electrons are ejected display a plateau, i.e., an intensity interval where the probability for ionization is almost constant. By analyzing the trajectories, we have confirmed that the majority of events for final charge states $\geq 3+$ in the intensity region $3 \times 10^{15} \leq I$ [W cm⁻²] $\leq 3 \times 10^{16}$ result from electron recollision. For the trajectories involving the ejection of three electrons (C^{3+} in the final state, cyan line with \times symbols in Fig. 2), the two valence electrons are ejected at one of the first local maxima of the electric field. One of the two ejected electrons later returns to the atomic core to knock out one of the inner valence electrons, resulting in a triply charged carbon ion. More interesting is the case when four electrons are ejected (C^{4+} in the final state, magenta line with $*$ symbols in Fig. 2). In this case, one of the ejected valence electrons comes back and knocks out two bound electrons, which results in a total of four free electrons after the laser pulse has passed.

Experimental evidence for recollision ionization in C was presented by Palaniyappan *et al.* in [92], where methane (CH₄) was exposed to intense laser light (800 nm, 35 fs). It was found that the ionization yield-vs-intensity curves for C^{4+} and C^{5+} exhibit clear plateau structures, indicative of a recollision mechanism. The laser intensity I_{plat} where the plateau starts

($I_{\text{plat}} \approx 10^{15}$ W/cm² for C⁴⁺ and $I_{\text{plat}} \approx 10^{16}$ W/cm² for C⁵⁺) [92] approximately agrees with our results in Fig. 2.

B. Quadruple ionization

For a detailed analysis of the trajectories leading to quadruple ionization, we fix the laser intensity to $I = 4 \times 10^{15}$ W/cm² in the following. At this particular intensity, we increase the total number of simulated trajectories to $k_{\text{tot}} = 8 \times 10^6$, in order to improve the statistics. A total number of $k_4 = 2702$ quadruple ionization trajectories were found.

As an aid to the analysis, we define the total energy ε_{ion} of the final C⁴⁺ ion (C nucleus + two bound electrons) as

$$\varepsilon_{\text{ion}} = \frac{\mathbf{P}^2}{2M} + \sum_b \varepsilon_b. \quad (9)$$

In Eq. (9), ε_b is the single-particle energy defined in Eq. (6), and the summation index b runs over the two electrons that are bound to the carbon nucleus in the final state. We furthermore define the total momentum of the ejected electrons as

$$\Phi = \sum_{\ell} \mathbf{p}_{\ell}, \quad (10)$$

where the sum runs over the four ejected electrons ℓ which have $\varepsilon_{\ell} > 0$ at the end of the simulation.

In Fig. 3(a), we show the distribution of the final values for ε_{ion} and the x component $\Phi_x = \hat{\mathbf{x}} \cdot \Phi$ of the total momentum, for trajectories leading to quadruple ionization. We recall that the electric field of the laser points in the x direction. Due to momentum conservation in the laser polarization direction, the final C⁴⁺ ion has momentum $-\Phi_x$. We note that usually it is the ion momentum, and not the total electron momentum, that is experimentally measured [9,11]. The distribution shown in Fig. 3(a) peaks at $\Phi_x \approx -12$ a.u., which is consistent with experimental results on other atoms [18]. The ponderomotive potential is $U_p \approx 9$ a.u. for our laser parameters, and $\sqrt{U_p} \approx 3$ a.u. The reason why only one peak at negative total momentum is observed is due to the short pulse used, so that recollision take place only once per laser pulse. For longer pulses, a momentum distribution symmetric around $\Phi_x = 0$ is expected. Furthermore, the position of the peak is expected to vary with the CEP φ_0 . For example, since a CEP of $\varphi_0 = \pi$ is equivalent to the case of $\varphi_0 = 0$ and $x \rightarrow -x$, a calculation with $\varphi_0 = \pi$ would lead to a distribution identical to that shown in Fig. 3(a), but with a peak at a positive value of the momentum.

As a function of ε_{ion} , the distribution in Fig. 3 has two peaks: one at $\varepsilon_{\text{ion}} \approx -32$ a.u., and one at $\varepsilon_{\text{ion}} \approx -24$ a.u. Moreover, the events belonging to the two peaks are correlated with the Φ_x value in the sense that trajectories with $\varepsilon_{\text{ion}} \approx -32$ a.u. have a smaller magnitude $|\Phi_x|$ of the momentum compared to the trajectories belonging to the peak at $\varepsilon_{\text{ion}} \approx -24$ a.u. To understand the two peaks in the distribution along ε_{ion} , we show Fig. 3(b). In this panel, we plot the distribution in Fig. 3(a) summed over the Φ_x direction [green, solid line in Fig. 3(b)]. The position of the two peaks around $\varepsilon_{\text{ion}} \approx -32$ a.u. and -24 a.u. can be understood by comparing with the vertical lines

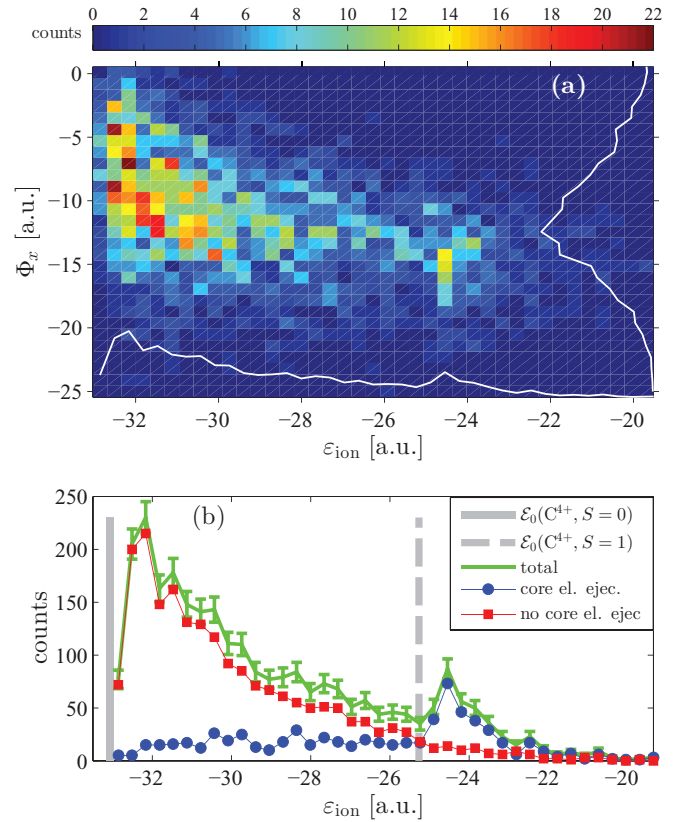


FIG. 3. (Color online) (a) Distribution of final bound-state energies ε_{ion} and final momentum Φ_x in the laser polarization direction, for quadruple ionization trajectories. The overlaid thin, solid lines represent the distribution summed over either ε_{ion} or Φ_x , on arbitrary scales. (b) Distribution of final bound-state energies ε_{ion} , divided into two groups: with and without core-electron ejection. The error bars on the total distribution show the estimated statistical error (one standard deviation). The vertical lines indicate the minimum energy of a C⁴⁺ ion with one α and one β electron (solid line), and a C⁴⁺ ion with two α electrons (dashed line). In both (a) and (b), the laser frequency is $\omega_0 = 0.057$ a.u., $\varphi_0 = 0$, and the intensity is $I = 4 \times 10^{15}$ W/cm².

(thick gray lines) in Fig. 3(b). The two vertical lines are drawn at $\mathcal{E}_0(S=0) = -33.062$ a.u. and $\mathcal{E}_0(S=1) = -25.265$ a.u. Here $\mathcal{E}_0(S=0)$ is the minimum energy of a C⁴⁺ ion (as described by the FMD model), where the two electrons have different spin (α and β), and the ion can be said to be in a state of total spin $S=0$. $\mathcal{E}_0(S=1)$ is the lowest possible energy for a C⁴⁺ ion with two electrons having the same spin ($\alpha\alpha$), and therefore $S=1$. For reference, we mention that the experimentally measured ground-state singlet-triplet difference in a real C⁴⁺ ion is $\mathcal{E}(^3S) - \mathcal{E}(^1S) = 10.99$ a.u. [93,94], to be compared with the FMD model $\mathcal{E}_0(S=1) - \mathcal{E}_0(S=0) = 7.80$ a.u.

The peak at $\varepsilon_{\text{ion}} \approx -32$ a.u. thus corresponds to a final C⁴⁺ ion in the $S=0$ state, while the peak at $\varepsilon_{\text{ion}} \approx -24$ a.u. corresponds to trajectories with a final C⁴⁺ ion in the $S=1$ state. We remark that since the FMD model is classical, there exists a continuous range of excited states above the ground state. For this reason, after the ejection of four electrons, the final C⁴⁺ ion never ends up in the exact ground state of minimum energy, but rather close, as can be

seen in Fig. 3(b). We also note that the ion kinetic-energy contribution $\mathbf{P}^2/(2M)$ to ε_{ion} is negligible due to the large value of M .

Two further curves (solid circles and solid squares) are plotted in Fig. 3(b). These distributions are obtained by sorting the trajectories leading to quadruple ionization according to whether one core electron is ejected or not. A core electron is defined as one of the two electrons i that has the smallest value of $\varepsilon_i \approx -13.8$ a.u. in the ground state [one of the electrons situated closest to the nucleus in Fig. 1(a)]. Since we keep track of the positions and momenta of all electrons during the calculation of a trajectory, it is straightforward to check for core-electron ejection at the end of each calculation by the criterion $\varepsilon_i > 0$ for either one of the core electrons. Trajectories where two core electrons are ejected were not found. The discussion about “core-electron ejection trajectories” below therefore refers to the situation where one core electron is ejected. In Fig. 3(b), we make two observations. The first is that core-electron ejection is not a rare event. Even at small final ion energies $\varepsilon_{\text{ion}} \approx -32$ a.u., core-electron ejection trajectories make up about 5% of the total number of the quadruple ionization trajectories. For final energies ε_{ion} above the $S = 1$ threshold of -25 a.u., a majority of the trajectories involve the ejection of one core electron. The second observation is that the peak at $\varepsilon_{\text{ion}} \approx -24$ a.u. in Fig. 3(b) contains mostly core ejection trajectories, which suggests that the final $S = 1$ states are formed by core-electron ejection. We have confirmed that all final states with $S = 1$ (two bound α electrons) are indeed the result of one core electron being ejected.

C. Examples of trajectories

In this section, we show examples of trajectories leading to quadruple ionization. The main focus is put on trajectories involving core-electron ejection, but a comparison with trajectories without core-electron ejection is also made. The core-electron ejection trajectories can be loosely divided into three categories, described in Table II.

TABLE II. Enumeration of the types of quadruple ionization trajectories involving core-electron ejection. In all three cases, the two valence electrons are first ejected at a field maximum by direct field ionization.

Category	Description
1	One inner valence electron and one core electron are ejected by a recolliding valence electron. The remaining inner valence electron then fills the vacant core hole.
2	Two inner valence electrons and one core electron are ejected by a recolliding valence electron. The vacant core hole is then filled by the recolliding valence electron, so that the initially ejected valence electron becomes recaptured.
3	One inner valence electron and one core electron having the same spin (both α or both β) are ejected by a recolliding valence electron, resulting in a final C^{4+} ion in a $S = 1$ state.

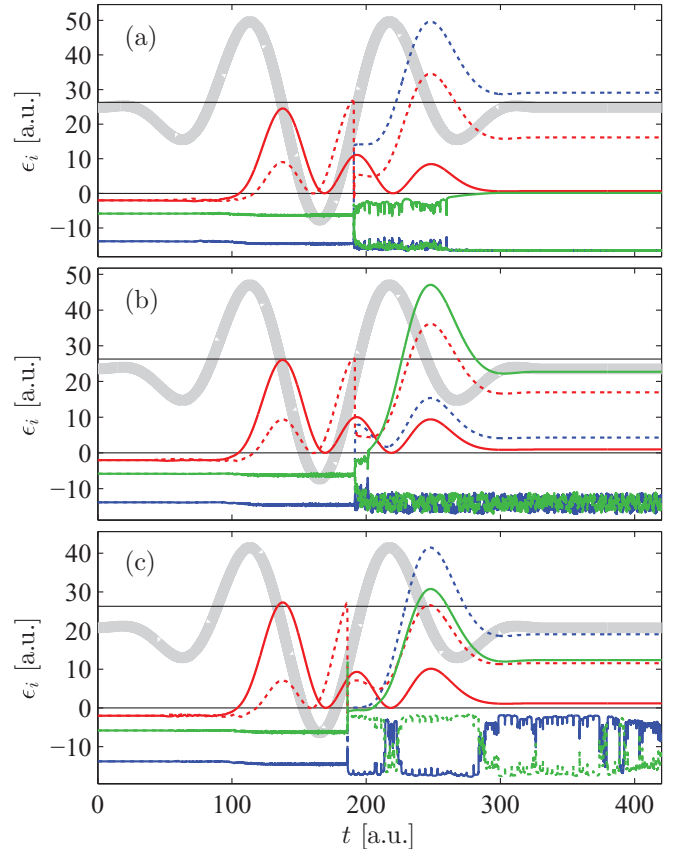


FIG. 4. (Color online) Recollision trajectories with core-electron ejection in category 1 (see Table II). The single-electron energies ε_i , $i = 1, 2, \dots, 6$, are shown as a function of time t . Spin α electrons are shown with solid lines and spin β electrons with broken lines. Red (gray) curves: valence electrons; green (light gray) curves: inner valence electrons; blue (black) curves: core electrons. For reference, solid, horizontal lines are drawn at $\varepsilon_i = 0$ and $\varepsilon_i = 3U_p \approx 26$ a.u. The laser field $\hat{\mathbf{x}} \cdot \mathbf{E}(t, \mathbf{0}) = E_0 \Psi(t)$ is shown (on an arbitrary scale) in the background with a thick line. The laser parameters are $\omega_0 = 0.057$ a.u. and $I = 4 \times 10^{15}$ W/cm² (same as in Fig. 3). The trajectory displayed in (a) has final bound energy $\varepsilon_{\text{ion}} = -33.0$ a.u., the trajectory in (b) has $\varepsilon_{\text{ion}} = -28.1$ a.u., and (c) has $\varepsilon_{\text{ion}} = -19.5$ a.u.

Examples of trajectories in category 1 with various values of the final bound energy ε_{ion} are shown in Fig. 4. In Fig. 4(a) we display a trajectory where there is a delay of about 100 a.u. (0.9 laser cycles) before the inner valence electron is ejected. This mechanism, where the recolliding electron excites a bound electron, which is later ejected is generally referred to as recollision excitation with subsequent ionization (RESI) [5, 6, 95–99]. We have checked that the ejection of the transiently bound electron is caused by field ionization, and not by autoionization. The trajectory calculation was repeated, without the laser field, starting from a point in time after the recollision, but before the ejection of the excited electron, e.g., from $t = 200$ a.u. in the case of the trajectory shown in Fig. 4(a). We confirmed that, in absence of the laser field, the excited electron was not ejected, but stayed bound. The final bound energy ε_{ion} of the trajectory in Fig. 4(a) is close to the ground-state energy $\mathcal{E}_0(S = 0) = -33.062$ a.u. of the C^{4+}

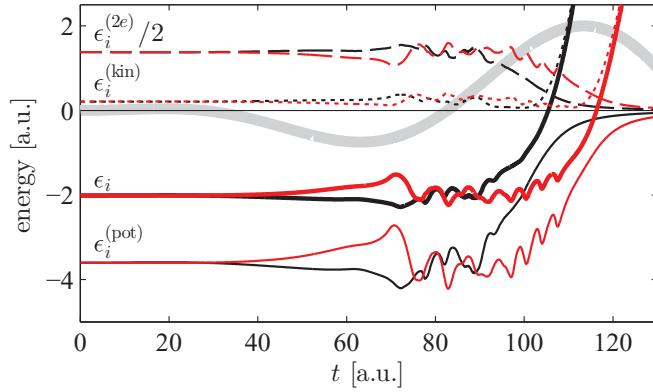


FIG. 5. (Color online) Contributions to the single-electron energy $\epsilon_i = \epsilon_i^{(\text{kin})} + \epsilon_i^{(\text{pot})} + \epsilon_i^{(\text{aux})} + \frac{1}{2}\epsilon_i^{(2e)}$ [see Eq. (6) for definition] for the two valence electrons [valence electron 1: red (gray) curves; valence electron 2: black curves]. For both electrons, $\epsilon_i^{(\text{aux})} < 0.04$ a.u. for all t , and $\epsilon_i^{(\text{aux})}$ is therefore not shown. The laser parameters and the initial conditions are the same as in Fig. 4(a). The laser field $\Psi(t)$ is shown (in arbitrary units) as a thick line in the background.

ion. The trajectories shown in Figs. 4(b) and 4(c) demonstrate that a range of final bound energies ϵ_{ion} are possible for the final C^{4+} ion. In Fig. 4(c), the two bound electrons are in a highly excited state, with the bound electrons repeatedly exchanging energy and switching roles of being the inner and outer electron. Note that, in Fig. 4(c), the final bound electrons have different spin. The highly excited C^{4+} ions formed in this way are stable, in the sense that they will not autoionize.

Before proceeding to the trajectories in category 2, we briefly discuss the ejection mechanism of the two valence electrons which are emitted close to a field maximum at $t \approx 100$ a.u. (see Fig. 4). Since quantum tunneling is not included in the FMD model, field ionization proceeds by absorption of enough energy from the laser field to overcome the threshold $\epsilon_i = 0$. In general, as has been pointed out in [100], the electron is excited to a bound, excited state before being emitted. We illustrate this statement in Fig. 5, where the different contributions to the single-electron energy are shown for the two valence electrons during the early part of the laser pulse. We can see that the two valence electrons absorb energy during the first laser cycle, while still being bound, and escape the binding potential at the end of the first cycle.

Figure 6 contains an example of trajectories from category 2, where the recolliding electron is trapped and becomes bound again after the recollision. To the best of our knowledge, the existence of this kind of trajectories has not been pointed out before in the context of NSMI. They are similar to a type of RESI trajectory found in the classical simulation of nonsequential double ionization in two-electron systems [40,49,101]: After knocking out a bound electron, the returning electron is trapped temporarily in an excited state before finally being emitted. Our simulations suggest that trajectories where the recolliding electron is trapped are not rare, at the intensity 4×10^{15} W/cm² considered in this section; about 11% of all quadruple ionization trajectories involve recapture of the recolliding electron. We also find that all trajectories where

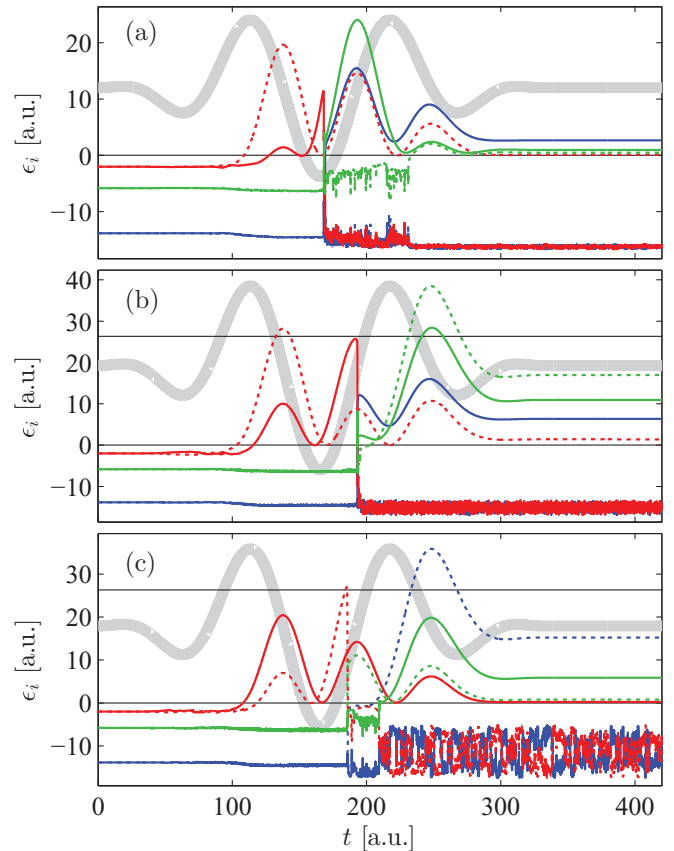


FIG. 6. (Color online) Recollision trajectories with core-electron ejection in category 2 (see Table II), recapture of the recolliding electron. The line styles and color coding of the curves are the same as in Fig. 4. The laser parameters are $\omega_0 = 0.057$ a.u. and $I = 4 \times 10^{15}$ W/cm². The trajectory shown in (a) has final bound energy $\epsilon_{\text{ion}} = -32.5$ a.u., the trajectory in (b) has $\epsilon_{\text{ion}} = -30.3$ a.u., and (c) has $\epsilon_{\text{ion}} = -22.6$ a.u.

the recolliding electron is recaptured also involve core-electron ejection. Apart from the recapture feature, the trajectories in Fig. 6 show similarities to those in Fig. 4 (category 1): there are trajectories where the last electron is ejected after some delay [Fig. 6(a); compare Fig. 4(a)], trajectories with a moderately excited final ion [Fig. 6(b); compare Fig. 4(b)], and trajectories with a highly excited C^{4+} ion in the final state [Fig. 6(c); compare Fig. 4(c)].

Trajectories from category 3 are demonstrated in Fig. 7. Here both electrons bound to the final C^{4+} have the same spin. Because of the spin-spin potential term $2\delta_{\sigma_i\sigma_j} f(q_{ij}, r_{ij}, \eta_0) r_{ij}^{-2}$ in the Hamiltonian (1), the bound electrons are forced to keep a certain distance between them; they cannot both be bound closely to the core. This can be clearly seen in Fig. 7(a). The probability for the production of $S = 1$ ions is high: for quadruple ionization trajectories with ion energies ϵ_{ion} above the $S = 1$ threshold $\mathcal{E}_0(S = 1) \approx -25.3$ a.u., 59% of all trajectories end up with a C^{4+} ion in the $S = 1$ state.

We conclude this section by showing in Fig. 8 two trajectories which do not involve core-electron ejection. The trajectory in Fig. 8(a) is similar to the trajectory shown in Fig. 4(a), with a delayed electron emission after recollision

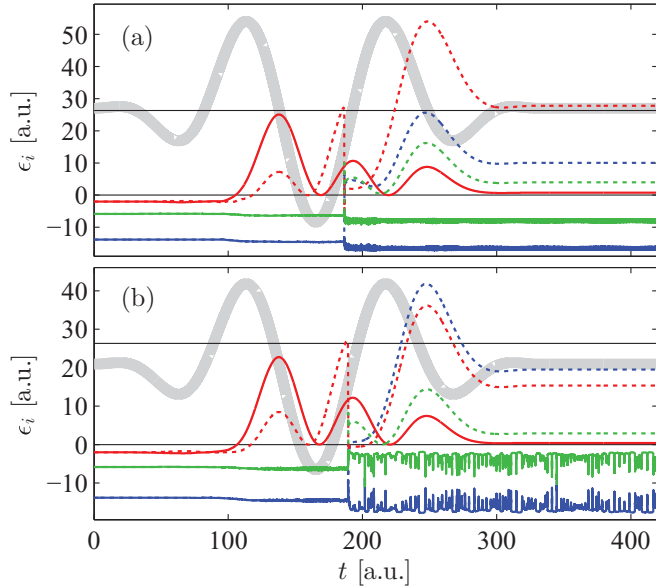


FIG. 7. (Color online) Recollision trajectories with core-electron ejection in category 3 (see Table II), where the bound electrons in the final state have equal spin. The line styles and color coding of the curves are the same as in Fig. 4, and the laser parameters are $\omega_0 = 0.057$ a.u. and $I = 4 \times 10^{15}$ W/cm². The trajectory in (a) has final bound energy $\epsilon_{\text{ion}} = -24.5$ a.u. and the trajectory in (b) has $\epsilon_{\text{ion}} = -19.7$ a.u.

and a final C⁴⁺ ion energy close to the ground-state energy. The trajectory shown in Fig. 8(b) resembles the trajectory in Fig. 6(c), with a highly excited final C⁴⁺ ion.

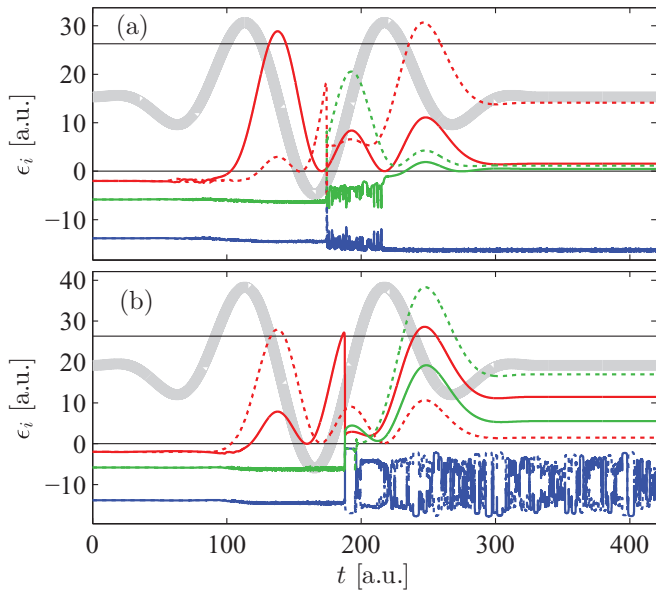


FIG. 8. (Color online) Recollision trajectories without core-electron ejection, where both core electrons stay bound. The line styles and color coding of the curves are the same as in Fig. 4, and the laser parameters are $\omega_0 = 0.057$ a.u. and $I = 4 \times 10^{15}$ W/cm². The trajectory in (a) has final bound energy $\epsilon_{\text{ion}} = -32.6$ a.u. and the trajectory in (b) has $\epsilon_{\text{ion}} = -19.8$ a.u.

IV. DISCUSSION AND SUMMARY

We have shown that the many-electron response of a carbon atom to an intense, few-cycle laser pulse can be described in a self-consistent way using the quasiclassical FMD model. Self-consistent means in this context that the complete time-dependent dynamics of the atom, from the unperturbed ground state to the laser-driven dynamics leading to recollision and a final, excited C⁴⁺ ion, can be simulated within one theoretical model. One of the main differences between the FMD model and other commonly employed, purely classical models [34–50,52–54] is that the FMD model gives rise to a shell structure of the neutral atom [62], meaning in a classical context that the minimum energy is accomplished by a configuration where the electrons are situated in pairs at different radial distances. This feature of the FMD model is exploited in the current paper to study the ejection of core electrons as a result of laser-induced recollisions.

The advantage of using a classical trajectory model is that new, unnoticed processes may be revealed by the analysis of a large number of trajectories. In the course of the current investigation, we found that recollision trajectories where the recolliding electron is trapped in a bound state after the recollision (see Fig. 6) are rather common, something which deserves further attention. Quantum mechanically, it is of course not possible to distinguish between a trajectory where the recolliding electron is trapped and a trajectory where the recolliding electron scatters inelastically, provided the electrons in the final states have the same momentum and energy [compare, for example, Figs. 4(a) and 6(a) or Figs. 4(b) and 6(b)]. However, our results suggest that Feynman diagrams representing such recapture trajectories may have to be included in *S*-matrix calculations of the nonsequential multiple-ionization process [5,6,102].

For experimental signatures of innershell ejection or core excitation, we note that fluorescence from a 3*s* innershell vacancy in Ar was measured in [103], and evidence for x-ray fluorescence arising from recollision-excited core electrons in Ne was observed in [104]. We suggest that, also in the present case of C atoms, excited C⁴⁺ ions could be experimentally verified by measuring the incoherent radiation due to the core relaxation. Representative decay rates in C⁴⁺ are $\Gamma \approx 3 \times 10^5$ s⁻¹ ($2^1S_0 \rightarrow 1^1S_0$, two-photon decay) [105], $\Gamma \approx 9 \times 10^{11}$ s⁻¹ ($2^1P_1 \rightarrow 1^1S_0$) [105], and $\Gamma \approx 5 \times 10^1$ s⁻¹ ($2^3S_1 \rightarrow 1^1S_0$) [105,106].

For few-cycle laser pulses, it is known that the recollision process is highly sensitive to the CEP of the laser pulse [107,108]. For this reason we expect the degree of core-electron ejection and the creation of excited core-hole states to vary as a function of the CEP. This could open up interesting possibilities where core-electron dynamics are controlled by the CEP of the laser pulse. As an experimental observable, one could measure the dependence on the CEP of the fluorescence from recollision-excited core-hole states.

ACKNOWLEDGMENTS

E.L. acknowledges support from the FPR program of RIKEN. The numerical calculations were carried out at the RIKEN Integrated Cluster of Clusters.

- [1] A. l'Huillier, L. A. Lompre, G. Mainfray, and C. Manus, *Phys. Rev. A* **27**, 2503 (1983).
- [2] D. N. Fittinghoff, P. R. Bolton, B. Chang, and K. C. Kulander, *Phys. Rev. Lett.* **69**, 2642 (1992).
- [3] K. Kondo, A. Sagisaka, T. Tamida, Y. Nabekawa, and S. Watanabe, *Phys. Rev. A* **48**, R2531 (1993).
- [4] B. Walker, B. Sheehy, L. F. DiMauro, P. Agostini, K. J. Schafer, and K. C. Kulander, *Phys. Rev. Lett.* **73**, 1227 (1994).
- [5] C. Figueira de Morisson Faria and X. Liu, *J. Mod. Opt.* **58**, 1076 (2011).
- [6] W. Becker, X. Liu, P. J. Ho, and J. H. Eberly, *Rev. Mod. Phys.* **84**, 1011 (2012).
- [7] M. Y. Kuchiev, *Pis'ma Zh. Eksp. Teor. Fiz.* **45**, 319 (1987) [*JETP Lett.* **45**, 404 (1987)].
- [8] P. B. Corkum, *Phys. Rev. Lett.* **71**, 1994 (1993).
- [9] S. Augst, A. Talebpour, S. L. Chin, Y. Beaudoin, and M. Chaker, *Phys. Rev. A* **52**, R917 (1995).
- [10] S. Larochelle, A. Talebpour, and S. L. Chin, *J. Phys. B* **31**, 1201 (1998).
- [11] R. Moshhammer, B. Feuerstein, W. Schmitt, A. Dorn, C. D. Schröter, J. Ullrich, H. Rottke, C. Trupp, M. Wittmann, G. Korn, K. Hoffmann, and W. Sandner, *Phys. Rev. Lett.* **84**, 447 (2000).
- [12] H. Maeda, M. Dammasch, U. Eichmann, W. Sandner, A. Becker, and F. H. M. Faisal, *Phys. Rev. A* **62**, 035402 (2000).
- [13] A. Rudenko, K. Zrost, B. Feuerstein, V. L. B. de Jesus, C. D. Schröter, R. Moshhammer, and J. Ullrich, *Phys. Rev. Lett.* **93**, 253001 (2004).
- [14] K. Yamakawa, Y. Akahane, Y. Fukuda, M. Aoyama, N. Inoue, H. Ueda, and T. Utsumi, *Phys. Rev. Lett.* **92**, 123001 (2004).
- [15] S. Palaniyappan, A. DiChiara, E. Chowdhury, A. Falkowski, G. Ongadi, E. L. Huskins, and B. C. Walker, *Phys. Rev. Lett.* **94**, 243003 (2005).
- [16] K. Zrost, A. Rudenko, T. Ergler, B. Feuerstein, V. L. B. de Jesus, C. D. Schröter, R. Moshhammer, and J. Ullrich, *J. Phys. B* **39**, S371 (2006).
- [17] S. Palaniyappan, A. DiChiara, I. Ghebregziabher, E. L. Huskins, A. Falkowski, D. Pajeroski, and B. C. Walker, *J. Phys. B* **39**, S357 (2006).
- [18] A. Rudenko, T. Ergler, K. Zrost, B. Feuerstein, V. L. B. de Jesus, C. D. Schröter, R. Moshhammer, and J. Ullrich, *J. Phys. B* **41**, 081006 (2008).
- [19] J. S. Parker, K. J. Meharg, G. A. McKenna, and K. T. Taylor, *J. Phys. B* **40**, 1729 (2007).
- [20] M. Lein and S. Kümmel, *Phys. Rev. Lett.* **94**, 143003 (2005).
- [21] F. Wilken and D. Bauer, *Phys. Rev. Lett.* **97**, 203001 (2006).
- [22] M. Thiele, E. K. U. Gross, and S. Kümmel, *Phys. Rev. Lett.* **100**, 153004 (2008).
- [23] J. Heslar, D. A. Telnov, and S.-I. Chu, *Phys. Rev. A* **87**, 052513 (2013).
- [24] T. Kato and H. Kono, *Chem. Phys. Lett.* **392**, 533 (2004).
- [25] T. Kato and H. Kono, *J. Chem. Phys.* **128**, 184102 (2008).
- [26] L. Greenman, P. J. Ho, S. Pabst, E. Kamarchik, D. A. Mazziotti, and R. Santra, *Phys. Rev. A* **82**, 023406 (2010).
- [27] D. Hochstuhl and M. Bonitz, *J. Chem. Phys.* **134**, 084106 (2011).
- [28] D. Hochstuhl and M. Bonitz, *Phys. Rev. A* **86**, 053424 (2012).
- [29] H. Miyagi and L. B. Madsen, *Phys. Rev. A* **87**, 062511 (2013).
- [30] T. Sato and K. L. Ishikawa, *Phys. Rev. A* **88**, 023402 (2013).
- [31] M. A. Lysaght, H. W. van der Hart, and P. G. Burke, *Phys. Rev. A* **79**, 053411 (2009).
- [32] M. A. Lysaght, S. Hutchinson, and H. W. van der Hart, *New J. Phys.* **11**, 093014 (2009).
- [33] S. Hutchinson, M. A. Lysaght, and H. W. van der Hart, *Phys. Rev. A* **88**, 023424 (2013).
- [34] R. Panfili, S. L. Haan, and J. H. Eberly, *Phys. Rev. Lett.* **89**, 113001 (2002).
- [35] P. J. Ho, R. Panfili, S. L. Haan, and J. H. Eberly, *Phys. Rev. Lett.* **94**, 093002 (2005).
- [36] P. J. Ho and J. H. Eberly, *Phys. Rev. Lett.* **95**, 193002 (2005).
- [37] S. L. Haan, J. S. Van Dyke, and Z. S. Smith, *Phys. Rev. Lett.* **101**, 113001 (2008).
- [38] X. Wang and J. H. Eberly, *Phys. Rev. Lett.* **103**, 103007 (2009).
- [39] Y. Zhou, Q. Liao, and P. Lu, *Phys. Rev. A* **80**, 023412 (2009).
- [40] F. Mauger, C. Chandre, and T. Uzer, *Phys. Rev. Lett.* **102**, 173002 (2009).
- [41] F. Mauger, C. Chandre, and T. Uzer, *J. Phys. B* **42**, 165602 (2009).
- [42] F. Mauger, C. Chandre, and T. Uzer, *Phys. Rev. Lett.* **104**, 043005 (2010).
- [43] F. Mauger, C. Chandre, and T. Uzer, *Phys. Rev. A* **81**, 063425 (2010).
- [44] X. Wang and J. H. Eberly, *Phys. Rev. Lett.* **105**, 083001 (2010).
- [45] A. Kamor, F. Mauger, C. Chandre, and T. Uzer, *Phys. Rev. E* **83**, 036211 (2011).
- [46] X. Wang and J. H. Eberly, *Phys. Rev. A* **86**, 013421 (2012).
- [47] X. Wang and J. H. Eberly, *J. Chem. Phys.* **137**, 22A542 (2012).
- [48] X. Wang, J. Tian, and J. H. Eberly, *Phys. Rev. Lett.* **110**, 073001 (2013).
- [49] E. Lötstedt and K. Midorikawa, *Phys. Rev. A* **87**, 013426 (2013).
- [50] Q. Tang, C. Huang, Y. Zhou, P. Lan, and P. Lu, *Phys. Rev. A* **89**, 053419 (2014).
- [51] R. Abrines and I. C. Percival, *Proc. Phys. Soc.* **88**, 861 (1966).
- [52] P. J. Ho and J. H. Eberly, *Phys. Rev. Lett.* **97**, 083001 (2006).
- [53] Y. Zhou, Q. Liao, and P. Lu, *Opt. Express* **18**, 16025 (2010).
- [54] Q. Tang, C. Huang, Y. Zhou, and P. Lu, *Opt. Express* **21**, 21433 (2013).
- [55] T. Brabec, M. Y. Ivanov, and P. B. Corkum, *Phys. Rev. A* **54**, R2551 (1996).
- [56] J. Chen, J. Liu, and W. M. Zheng, *Phys. Rev. A* **66**, 043410 (2002).
- [57] D. F. Ye, X. Liu, and J. Liu, *Phys. Rev. Lett.* **101**, 233003 (2008).
- [58] M. Y. Wu, Y. L. Wang, X. J. Liu, W. D. Li, X. L. Hao, and J. Chen, *Phys. Rev. A* **87**, 013431 (2013).
- [59] M. V. Ammosov, N. B. Delone, and V. P. Kraĭnov, *Zh. Eksp. Teor. Fiz.* **91**, 2008 (1986) [*Sov. Phys. JETP* **64**, 1191 (1986)].
- [60] L. Wilets, E. Henley, M. Kraft, and A. Mackellar, *Nucl. Phys. A* **282**, 341 (1977).
- [61] C. L. Kirschbaum and L. Wilets, *Phys. Rev. A* **21**, 834 (1980).
- [62] J. S. Cohen, *Phys. Rev. A* **51**, 266 (1995).
- [63] J. S. Cohen, *Phys. Rev. A* **57**, 4964 (1998).
- [64] D. Zajfman and D. Maor, *Phys. Rev. Lett.* **56**, 320 (1986).
- [65] W. A. Beck, L. Wilets, and M. A. Alberg, *Phys. Rev. A* **48**, 2779 (1993).
- [66] J. S. Cohen, *Phys. Rev. A* **56**, 3583 (1997).
- [67] W. A. Beck and L. Wilets, *Phys. Rev. A* **55**, 2821 (1997).
- [68] J. S. Cohen, *Phys. Rev. A* **59**, 4300 (1999).

- [69] J. S. Cohen, *Phys. Rev. A* **59**, 1160 (1999).
- [70] J. S. Cohen, *J. Phys. B* **38**, 441 (2005).
- [71] J. S. Cohen, *J. Phys. B* **39**, 3561 (2006).
- [72] J. S. Cohen, *J. Phys. B* **39**, 1517 (2006).
- [73] P. B. Lerner, K. J. LaGattuta, and J. S. Cohen, *Laser Phys.* **3**, 331 (1993).
- [74] K. J. LaGattuta and J. S. Cohen, *J. Phys. B* **31**, 5281 (1998).
- [75] D. A. Wasson and S. E. Koonin, *Phys. Rev. A* **39**, 5676 (1989).
- [76] K. J. LaGattuta, *J. Phys. B* **33**, 2489 (2000).
- [77] Y. Zhou, C. Huang, Q. Liao, and P. Lu, *Phys. Rev. Lett.* **109**, 053004 (2012).
- [78] Y. Zhou, C. Huang, and P. Lu, *Opt. Express* **20**, 20201 (2012).
- [79] Y. Zhou, Q. Zhang, C. Huang, and P. Lu, *Phys. Rev. A* **86**, 043427 (2012).
- [80] K. J. LaGattuta, *Phys. Rev. A* **73**, 043404 (2006).
- [81] E. Lötstedt, T. Kato, and K. Yamanouchi, *Phys. Rev. Lett.* **106**, 203001 (2011).
- [82] C. Huang, Z. Li, Y. Zhou, Q. Tang, Q. Liao, and P. Lu, *Opt. Express* **20**, 11700 (2012).
- [83] E. Lötstedt, T. Kato, and K. Yamanouchi, *Phys. Rev. A* **85**, 053410 (2012).
- [84] D. Bauer, *J. Phys. B* **37**, 3085 (2004).
- [85] L. Wilets and J. S. Cohen, *Contemp. Phys.* **39**, 163 (1998).
- [86] K. J. LaGattuta, *J. Phys. A* **36**, 6013 (2003).
- [87] J. A. Nelder and R. Mead, *Comput. J.* **7**, 308 (1965).
- [88] W. H. Press, S. A. Teukolsky, W. T. Vetterling, and B. P. Flannery, *Numerical Recipes in Fortran 77: The Art of Scientific Computing* (Cambridge University Press, Cambridge, UK, 1992).
- [89] T. Koopmans, *Physica* **1**, 104 (1934).
- [90] M. W. Schmidt, K. K. Baldridge, J. A. Boatz, S. T. Elbert, M. S. Gordon, J. H. Jensen, S. Koseki, N. Matsunaga, K. A. Nguyen, S. Su, T. L. Windus, M. Dupuis, and J. A. Montgomery, Jr., *J. Comput. Chem.* **14**, 1347 (1993).
- [91] K. L. Bell, H. B. Gilbody, J. G. Hughes, A. E. Kingston, and F. J. Smith, *J. Phys. Chem. Ref. Data* **12**, 891 (1983).
- [92] S. Palaniyappan, R. Mitchell, R. Sauer, I. Ghebregziabher, S. L. White, M. F. Decamp, and B. C. Walker, *Phys. Rev. Lett.* **100**, 183001 (2008).
- [93] A. Kramida, Yu. Ralchenko, J. Reader, and NIST ASD Team, NIST Atomic Spectra Database (ver. 5.1) (online). Available at <http://physics.nist.gov/asd> (National Institute of Standards and Technology, Gaithersburg, MD, 2013).
- [94] L. Engstrom, P. Bengtsson, C. Jupen, and M. Westerlind, *J. Phys. B* **25**, 2459 (1992).
- [95] H. W. van der Hart and K. Burnett, *Phys. Rev. A* **62**, 013407 (2000).
- [96] G. L. Yudin and M. Y. Ivanov, *Phys. Rev. A* **63**, 033404 (2001).
- [97] B. Feuerstein, R. Moshhammer, D. Fischer, A. Dorn, C. D. Schröter, J. Deipenwisch, J. R. Crespo Lopez-Urrutia, C. Höhr, P. Neumayer, J. Ullrich, H. Rottke, C. Trumpf, M. Wittmann, G. Korn, and W. Sandner, *Phys. Rev. Lett.* **87**, 043003 (2001).
- [98] S. L. Haan, L. Breen, A. Karim, and J. H. Eberly, *Phys. Rev. Lett.* **97**, 103008 (2006).
- [99] T. Shaaran, M. T. Nygren, and C. Figueira de Morisson Faria, *Phys. Rev. A* **81**, 063413 (2010).
- [100] K. LaGattuta, *Opt. Express* **8**, 401 (2001).
- [101] S. L. Haan, L. Breen, A. Karim, and J. H. Eberly, *Opt. Express* **15**, 767 (2007).
- [102] A. Becker and F. H. M. Faisal, *J. Phys. B* **38**, R1 (2005).
- [103] A. Becker, F. H. M. Faisal, Y. Liang, S. Augst, Y. Beaudoin, M. Chaker, and S. L. Chin, *J. Phys. B* **33**, L547 (2000).
- [104] G. Marcus, W. Helml, X. Gu, Y. Deng, R. Hartmann, T. Kobayashi, L. Strueder, R. Kienberger, and F. Krausz, *Phys. Rev. Lett.* **108**, 023201 (2012).
- [105] C. D. Lin, W. R. Johnson, and A. Dalgarno, *Phys. Rev. A* **15**, 154 (1977).
- [106] H. T. Schmidt, P. Forck, M. Grieser, D. Habs, J. Kenntner, G. Miersch, R. Repnow, U. Schramm, T. Schüssler, D. Schwalm, and A. Wolf, *Phys. Rev. Lett.* **72**, 1616 (1994).
- [107] X. Liu and C. Figueira de Morisson Faria, *Phys. Rev. Lett.* **92**, 133006 (2004).
- [108] B. Bergues, M. Kübel, N. G. Johnson, B. Fischer, N. Camus, K. J. Betsch, O. Herrwerth, A. Senftleben, A. M. Saylor, T. Rathje, T. Pfeifer, I. Ben-Itzhak, R. R. Jones, G. G. Paulus, F. Krausz, R. Moshhammer, J. Ullrich, and M. F. Kling, *Nat. Commun.* **3**, 813 (2012).